Available online www.jsaer.com

***Journal of Scientific and Engineering Research*, 2024, 11(4):197-208**

Research Article

ISSN: 2394-2630
CODEN(USA): JSERBR

Spectral investigation; Electronic structure calculations on 4-chlorophenyl-4-chlorobenzenesulfonate

M. Govindarajan[a,b]

[a]Department of Physics, AGCW College, Karaiakal, Puduherry, India
[b]Department of Physics, AAGAS College, Karaiakal, Puduherry, India
Tel: +91-9443525988
Email: govindarajan64@gmail.com

Abstract In this work, the vibrational spectral analysis was carried out by using FT-Raman and FT-IR spectroscopy in the range 100-4000 cm^{-1} and 400-4000 cm^{-1} respectively, for 4-chlorophenyl-4-chlorobenzenesulfonate (4CLPH4CLBENSUL) molecule. The potential energy curve shows that 4CLPH4CLBENSUL molecule has two stable structures. The computational results diagnose the most stable conformer of the 4CLPH4CLBENSUL as the S1 structure. The molecular structure, fundamental vibrational frequencies and intensity of the vibrational bands were interpreted with the aid of structure optimizations and normal coordinate force field calculations based density functional theory (DFT) and ab initio HF methods and different basis sets combination. The complete vibrational assignments of wavenumbers were made on the basis of potential energy distribution (PED). The energy and oscillator strength calculated by Time-Dependent Density Functional Theory (TD-DFT) complements with the experimental findings. In addition, molecular electrostatic potential, nonlinear optical and thermodynamic properties of the title compound were performed. Mulliken and natural charges of the title molecule were also calculated and interpreted.

Keywords on 4-chlorophenyl-4-chlorobenzenesulfonate; FT-IR; FT-RAMAN; HOMO-LUMO; DFT/B3LYP and HF.

1. Information for healthcare professionals

Onychomycosis can be difficult to diagnose based on physical appearance and clinical history alone. Clinicians should confirm a diagnosis of onychomycosis by laboratory testing before prescribing antifungal medications [1, 2]. Potassium hydroxide stain is prepared the official document, but the accuracy of the test depends on clinician feel and proficiency. Nail cuttings or scrapings are located in a drop of KOH and analysed under a microscope for the presence of fungal elements [3]. Histopathologic examination with a periodic acid-Schiff (PAS) stain: Examination of nail clippings with a PAS stain can confirm the diagnosis of a fungal nail infection. Culture: Fungal culture can be used to identify the infecting organism, but the fungi may take several weeks to grow [4-8]. Molecular: Molecular testing, including polymerase chain reaction (PCR) testing, may be used to diagnose fungal nail infections. Antimicrobial-resistant onychomycosis is a growing problem [9-15]. Therefore, antifungal susceptibility testing may be considered based on the fungus or fungi identified and the patient's clinical course [16, 17].

2. Experimental details

The compound under investigation namely 4CLPH4CLBENSUL is purchased from Sigma-Aldrich chemicals, U.S.A with spectroscopic grade and it was used as such without any further purification. The FT-IR spectrum of the compound has been recorded in Perkin-Elmer 180 Spectrometer in the range of 400–4000 cm^{-1}. The spectral resolution is ± 2 cm^{-1}. The FT-Raman spectrum of the compound was also recorded in the same instrument with FRA 106 Raman module equipped with Nd: YAG laser source operating in the region 100-4000 cm^{-1} at 1.064 μm line widths with 200 mW powers. The spectra were recorded with scanning speed of 30 cm^{-1} min^{-1} of spectral width 2cm^{-1}. The frequencies of all sharp bands are accurate to ± 1 cm^{-1}

3. Quantum chemical calculations

The entire quantum chemical calculations have been performed at DFT (B3LYP) and ab-initio HF methods with 6-311++G(d,p) basis set using the Gaussian 09 program [18]. The optimized structural parameters have been evaluated for the calculations of vibrational frequencies at different level of theories and a variety of basis sets by assuming C_S point group symmetry. At the optimized geometry for the title molecule no imaginary frequency modes were obtained, therefore a true minimum on the potential energy surface was found. As a result, the unscaled calculated frequencies, reduced masses, force constants, infrared intensities, Raman activities, Raman intensities, and depolarization ratios were obtained. In order to improve the calculated values in agreement with the experimental values, a spectral uniform scaling factor was used to offset the systematic errors caused by basis set incompleteness, neglect of electron correlation and vibrational anharmonicity. Hence, the vibrational frequencies calculated at HF level are scaled by 0.905 [19] and the range of wave numbers above 1700 cm^{-1} are scaled as 0.958 and below 1700 cm^{-1} scaled as 0.983 for B3LYP/6-311++G(d,p) [22,21]. After scaled with the scaling factor, the deviation from the experiments is less than 10 cm^{-1} with a few exceptions. Gauss view program [22, 23] has been considered to get visual animation and also for the verification of the normal modes assignment.

The electronic absorption spectra for optimized molecule calculated with time dependent density functional theory (TD-DFT) at B3LYP/6-311++G(d,p) level. To investigate the reactive sites of the title compound the molecular electrostatic potential was evaluated. Furthermore, in order to show nonlinear optic (NLO) activity of 4CLPH4CLBENSUL molecule, the dipole moment, linear polarizability and first hyperpolarizability were obtained from molecular polarizabilities based on theoretical calculations. Moreover, the changes in the thermodynamic functions (the heat capacity, entropy, and enthalpy) were investigated for the different temperatures from the vibrational frequency calculations of title molecule.

3.1 Prediction of Raman intensities

The Raman activities (S_{Ra}) calculated with Gaussian 03 program converted to relative Raman intensities (I_{Ra}) using the following relationship derived from the intensity theory of Raman scattering [30,31]:

$$I_i = \frac{f\left(\nu_0 - \nu_i\right)^4 S_i}{\nu_i\left[1 - \exp\left(-hc\nu_i / kT\right)\right]}$$

where; ν_0 is the laser exciting wavenumber in cm^{-1} (in this work, we have used the excitation wavenumber ν_0 = 9398.5 cm^{-1}, which corresponds to the wavelength of 1064 nm of a Nd:YAG laser), ν_i the vibrational wavenumber of the i^{th} normal mode (cm^{-1}), while S_i is the Raman scattering activity of the normal mode ν_i. f (is a constant equal to 10^{-12}) is a suitably chosen common normalization factor for all peak intensities. h, k, c and T are Planck and Boltzmann constants, speed of light and temperature in Kelvin, respectively.

4. Results and Discussion

4.1 Potential energy surface (PES) scan, conformational isomers and molecular geometry

The 4CLPH4CLBENSUL has one substituent group (sulfonate and oxygen group) attached to two planar different rings. The sulfonate and oxygen was chosen to investigate the possible conformers of the 4CLPH4CLBENSULmolecule.In order to describe conformational flexibility of the title molecule, the energy profile as a function of C–S–O–C (SC1) and C-C-S-O (SC2) dihedral angle were achieved with PM6 method

(Fig. 1a). All the geometrical parameters were simultaneously relaxed during the calculations while the dihedral angles were varied in steps of 10^0. As can be seen from Fig. 1a, the local minima at 0^0 (or 360^0) and 180^0 were obtained for 121 conformers, respectively. These result show that 4CLPH4CLBENSULmolecule have two possible structures; depend on the positions of the sulfonate atom bonded to oxygen, whether it is directed away from or toward the ring. Similarly, the energy profiles as a function of dihedral angle were achieved with PM6 method (Fig. 1b). As can be seen from Fig. 1, the most stable conformer is for SC2 with energy -0.137213. The optimized geometry of the molecule is yielded only one conformer at this stage. The resulted potential energy curve is depicted in Fig. 1b show form for minimum energy. Both forms of the molecule are in the same plane. In this study, calculations were done for two molecular views of title molecule, however, tables and figures were prepared only for the most stable conformer.

The theoretical possible optimized geometric structure with atoms numbering of 4-chlorophenyl-4-chlorobenzenesulfonate is shown in Fig. 1b. The internal coordinates describe the position of the atoms in terms of distances, angles and dihedral angles with respect to an origin atom. The symmetry coordinates are constructed using the set of internal coordinates. By allowing the relaxation of all parameters, the calculations converge to optimized geometries, which correspond to true energy minima, as revealed by the lack of imaginary frequencies in the vibrational mode calculation.

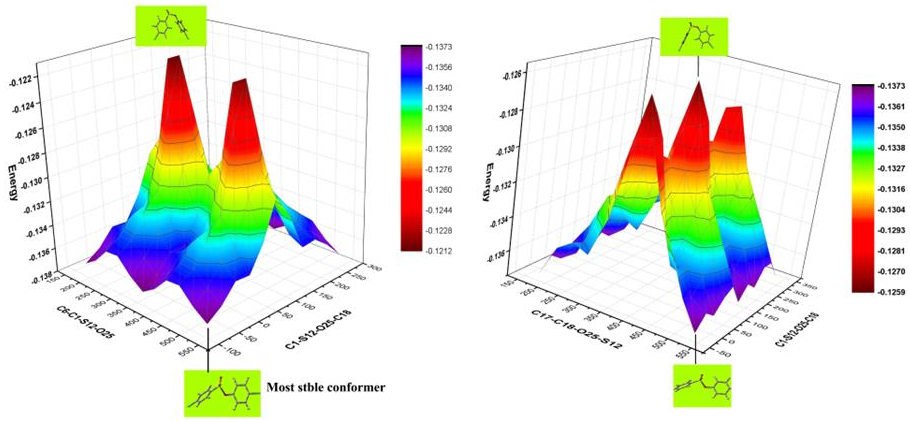

Figure 1: PES scan for the selected degree, T(C-S-O-C) and T(C-C-S-O) torsional freedom

Table 1: Optimized parameters (bond length and bond angle) of 4CLPH4CLBENSUL

Bond length	HF	B3LYP	Experimental value [23]
R(C1,C2)	1.3853	1.3952	1.379
R(C1,C6)	1.3854	1.3954	1.411
R(C1,S12)	1.7581	1.7822	
R(C2,C3)	1.3823	1.3926	1.377
R(C2,H7)	1.0732	1.0841	0.9300
R(C3,C4)	1.3845	1.3963	1.398
R(C3,H8)	1.073	1.0838	0.9300
R(C4,C5)	1.3845	1.3964	1.374
R(C4,Cl11)	1.7366	1.7515	1.741
R(C5,C6)	1.3823	1.3925	1.382
R(C5,H9)	1.073	1.0838	0.9300
R(C6,H10)	1.0732	1.0841	0.9300
R(S12,O13)	1.4237	1.4604	1.450
R(S12,O14)	1.4237	1.4601	1.451
R(S12,O25)	1.5986	1.6759	1.462
R(C15,C16)	1.3832	1.3951	1.370
R(C15,C20)	1.3832	1.3951	
R(C15,Cl26)	1.7417	1.7572	1.745
R(C16,C17)	1.3839	1.3939	1.370
R(C16,H21)	1.0732	1.0839	0.9600
R(C17,C18)	1.3794	1.3933	1.397

R(C17,H22)	1.073	1.0836	0.9600
R(C18,C19)	1.3794	1.393	1.370
R(C18,O25)	1.3929	1.4037	0.9600
R(C19,C20)	1.3839	1.3937	1.402
R(19,H23)	1.073	1.0837	0.9600
R(C20,H24)	1.0732	1.0839	
Bond angle	HF	B3LYP	
A(C2,C1,C6)	121.4083	121.7227	118.6
A(C2,C1,S12)	119.295	119.0859	119.6
A(C6,C1,S12)	119.2935	119.1843	121.6
A(C1,C2,C3)	119.3181	119.1496	121.9
A(C1,C2,H7)	120.1891	120.0638	119.1
A(C3,C2,H7)	120.4882	120.7825	119.1
A(C2,C3,C4)	119.1616	119.181	118.3
A(C2,C3,H8)	120.637	120.6963	120.8
A(C4,C3,H8)	120.2006	120.122	120.8
A(C3,C4,C5)	121.6293	121.615	121.5
A(C3,C4,Cl11)	119.1861	119.1947	
A(C5,C4,Cl11)	119.1838	119.1895	
A(C4,C5,C6)	119.1622	119.1831	119.4
A(C4,C5,H9)	120.1981	120.1187	120.3
A(C6,C5,H9)	120.6389	120.6974	120.3
A(C1,C6,C5)	119.3175	119.1451	118.6
A(C1,C6,H10)	120.1869	120.1161	119.8
A(C5,C6,H10)	120.4911	120.7347	119.8
A(C1,S12,O13)	109.7628	109.7519	
A(C1,S12,O14)	109.7632	109.7985	
A(C1,S12,O25)	98.5516	96.9829	
A(O13,S12,O14)	120.2313	120.9397	
A(O13,S12,O25)	108.1569	108.3208	
A(O14,S12,O25)	108.155	108.3561	
A(C16,C15,C20)	121.2169	121.3502	
A(C16,C15,Cl26)	119.3916	119.3307	
A(C20,C15,Cl26)	119.3915	119.3192	
A(C15,C16,C17)	119.4053	119.305	
A(C15,C16, H21)	120.1774	120.1344	
AC(17,C16,H21)	120.4172	120.5606	
A(C16,C17,C18)	119.0651	119.2631	
A(C16,C17,H22)	121.045	121.0417	
A(C18,C17,H22)	119.8892	119.6951	
A(C17,C18,C19)	121.8418	121.4983	
A(C17,C18,H25)	119.0477	119.4166	
A(C19,C18,H25)	119.0484	119.0172	
A(C18,C19,C20)	119.0644	119.3052	
A(C18,C19,H23)	119.8897	119.6628	
A(C20,C19,H23)	121.0452	121.032	
A(C15,C20,C19)	119.4061	119.2764	
A(C15,C20,H24)	120.1771	120.1399	
A(C19,C20,H24)	120.4167	120.5836	
A(S12,O25,C18)	118.8836\	116.1342	
C1,C2,C3,C4,C5,C6,H7,H8,H9,H10,Cl11,S12,O13,O14,C15,C16,C17,C18,C19,C20,H21,H22,H23,H24,O25,Cl 26			

[23] reference number

The optimized bond lengths, bond angles and experimental values of this compound are calculated by HF and DFT/B3LYP methods with 6-31+G(d,p) is listed in Table 1 for S2 form of 4CLPH4CLBENSUL [24]. Ground state bond angles and dihedral angles data suggest that the OH group of 4CLPH4CLBENSULis the same plane that of the ring. The optimized structure of the molecule is shown in the Fig .2. From the calculations, the

optimized structure of 4CLPH4CLBENSULwas calculated to exist in a planar structure. The bond distances evaluated by B3LYP method were larger than obtained by HF and PM3 methods. This molecule has one S-O, one C-S, two C-Cl, three S-O, eight C-H and twelve C-C bond lengths. The B3LYP/6-31+G(d,p) method overestimates bond lengths, particularly the C-H bond lengths. Researchers have explained the changes in the frequency, bond length or bond angle of C–H bond on substitution due to a change in the charge distribution on the carbon atom of the ring. In substituted ring, the ring carbon atoms exert a large attraction on the valence electron cloud of the H atom resulting in an increase in the C–H force constant and a decrease in the corresponding bond length. In the present work, the C–H bond lengths were calculated as 1.08395 Å in B3LYP/6-31++(d,p) and 1.073 Å in HF/6-31+(d,p). The HF C-H bond length values are mostly coincided with the experimental values. But, the B3LYP values are little bit far away from the experimental values. The C-C bond distances of 4CLPH4CLBENSUL are found to have higher values in case of B3LYP calculation with respect to other basis computation. But the experimental values C1-C6 are C3-C4, C17-C18 and C19-C20 little bit beyond the B3LYP values. The remaining experimental values are below HF values. The higher most value C-C bond length is calculated in C4-C5 in B3LYP/6-31+G(d,p). The differences between the C–Cl bond distances are very high. The values bond lengths C4-Cl11 and C15-Cl26 are 1.741 and 1.745 Å. The S–O bond lengths were found 1.4604, 1.4601 and 1.6759Å B3LYP/6-31+G(d,p) and 1.4237 and 1.5986Å HF/6-31+G(d,p).The optimized bond lengths of title moleculeatB3LYP/6-311++G(d,p) is shown in Fig. 3. Compared with the B3LYP, the HF approach is applied to less estimate the bond lengths.

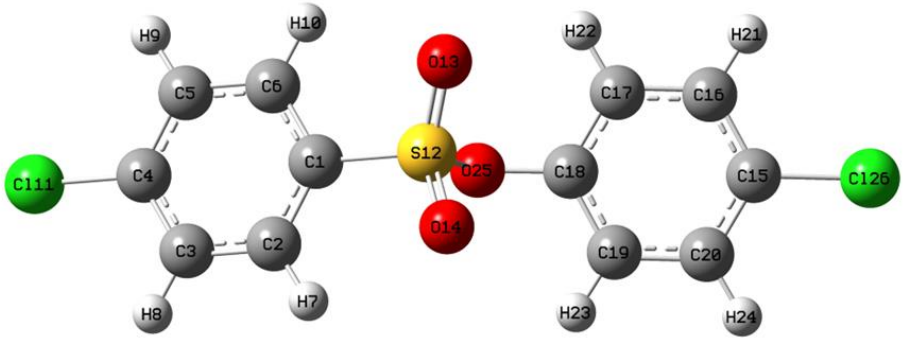

Figure 2: The theoretical possible optimized geometric structures with atoms numbering of 4CLPH4CLBENSUL

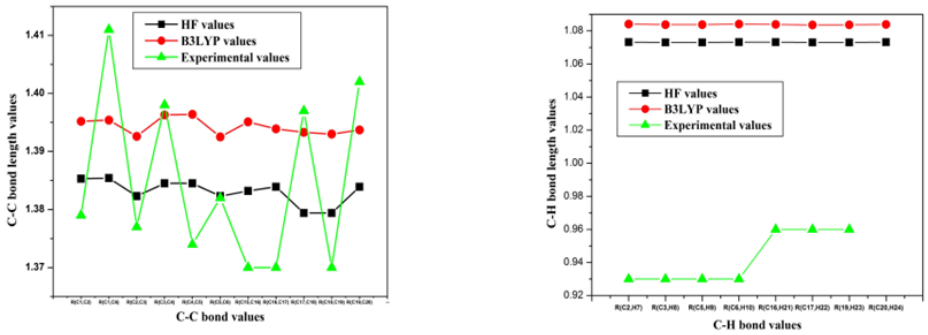

Figure 3: The optimized bond lengths C-C and C-H of title molecule.

The DFT calculation gives decrease of angles C1–C2–C3 and C4–C5–C6 and increase of angle C2–C1–C6, C2–C3–C4and C1–C6–C5. In this molecule, the largest deviation of the torsion angle N12–C8–N13 with B3LYP/6-311++G(d,p) is 7.8°. The calculated bond angle values suggest that the ring of the molecule is distorted due to the steric and electronic effects.

4.2 Mulliken and Natural charge distribution

The Mulliken charge is related to the vibrational quantum analysis of the molecule, and quantifies how the electronic nature structure changes under atomic displacement; it is therefore related directly to the chemical properties present in the molecule [25]. The Mulliken and natural charge distribution of the molecule are calculated on HF and B3LYP levels with basis sets. The calculated values of the charges of title molecule at gaseous phase are given in Table 2. The Mulliken and natural charge distribution of 4CLPH4CLBENSUL structurally and graphically are shown in Figs. 4 (a) and (b). All carbon atoms are moderate except one carbon C18 high value and low value one carbon atom C1. All the carbon atoms are having negative value expect C18. Among all the atoms, sulpher atom is having the highest value and lower value is oxygen atom mulliken charge. The three oxygen atoms O25 is the lowest value. The Cl values of mulliken charge are nearer to zero value. The charge distribution of the title compound shows that the carbon atom attached with hydrogen atoms is negative. In both Mulliken and natural charges are not shows more deviations with other hydrogen atoms and they are having the medium positive value. The maximum Mulliken and natural charge 0.345029 and 0.49628 are obtained for atom H15 with HF method using 6-311G++(d,p) and 6-311G(d,p) sets, respectively. This is due to the attachment of negatively charged chlorine atoms. The natural and Mulliken charges all hydrogen atoms are positive.

Table 2: Mulliken and Natural charge distribution of 4CLPH4CLBENSUL

Atoms	Milliken charges		Natural charges	
	B3LYP	HF	B3LYP	HF
C1	-0.189212	-0.352731	-0.32967	-0.38030
C2	-0.065987	-0.085264	-0.13994	-0.09222
C3	-0.067609	-0.120892	-0.22038	-0.23344
C4	-0.087544	-0.144156	-0.00651	0.03454
C5	-0.067715	-0.120887	-0.22013	-0.23315
C6	-0.064628	-0.085280	-0.13935	-0.09141
H7	0.145263	0.214574	0.24133	0.23292
H8	0.128436	0.194229	0.23102	0.22238
H9	0.128499	0.194228	0.23108	0.22243
H10	0.144683	0.214588	0.24049	0.23181
Cl11	0.008520	0.027931	0.03634	0.00990
S12	1.252773	1.693292	2.29616	2.50620
O13	-0.510070	-0.657212	-0.89841	-0.99217
O14	-0.508828	-0.657227	-0.87929	-0.97599
C15	-0.085743	-0.160538	-0.03893	-0.03505
C16	-0.083660	-0.119772	-0.20385	-0.17637
C17	-0.062230	-0.120501	-0.25201	-0.25308
C18	0.278314	0.315090	0.30808	0.35323
C19	-0.062433	-0.120499	-0.22019	-0.21827
C20	-0.083625	-0.119772	-0.21078	-0.18342
H21	0.119708	0.187959	0.21993	0.20964
H22	0.121409	0.193820	0.24698	0.24253
H23	0.117636	0.193836	0.22346	0.21328
H24	0.119356	0.187958	0.21939	0.20867
O25	-0.611229	-0.761926	-0.72646	-0.79054
Cl26	-0.014083	0.009152	-0.00836	-0.03213

Table 3: Thermodynamic properties at different temperatures at the B3LYP/6-311++G(d,p) level for 4CLPH4CLBENSUL

Temperature	C Heat capacity	S Entropy	H Enthalpy
100	22.587	86.069	1.393
200	39.061	106.362	6.964
298.15	53.477	125.955	13.091
400	70.203	146.823	18.433
500	85.605	166.392	24.921
600	92.185	181.30	35.238
700	98.318	195.646	45.513
800	104.690	210.300	57.016
900	111.141	225.035	67.654
1000	118.24	239.113	78.277

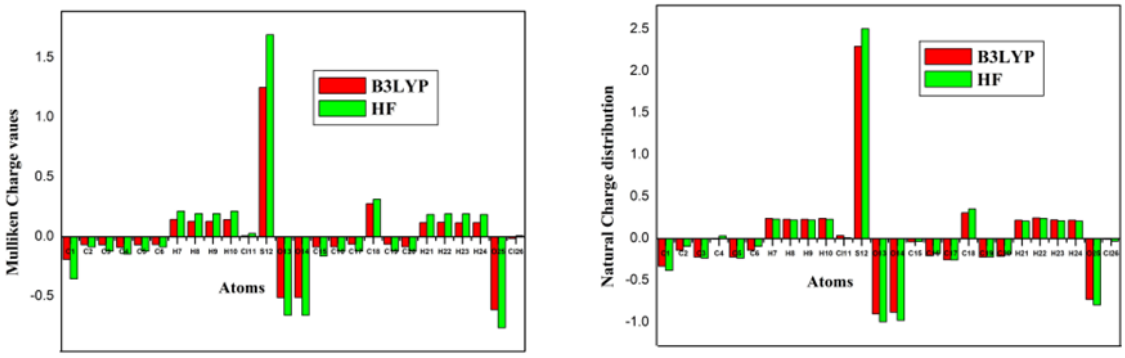

Figure 4: The Mulliken and Natural charge distribution of 4CLPH4CLBENSUL

4.3 Thermodynamic Properties

Some calculated thermodynamic parameters (such as zero-point vibrational energy, thermal energy, specific heat capacity, rotational constants, entropy, and dipole moment) of 4CLPH4CLBENSUL by DFT/B3LYP and HF methods at 298.15 K and 1.00 atm pressure were listed in Table 3. The global minimum energy obtained for structure optimization of 4CLPH4CLBENSUL are ca. -2006.2889 a.u, and -2000.0769 a.u for B3LYP and HF methods with 6-31+G(d,p) basis sets. All the above observations were made without any symmetric constrains. The rotational constants are decreasing in values from HF to B3LYP method and nearly equal in HF methods. Entropy values are higher in B3LYP/6-311+G(d,p) in comparison with other basis sets. The thermal energies are also in the same trend with global minimum energy. The lowermost thermal energy is observed 22.587kcal mol^{-1} in B3LYP/6-31G+(d,p). The total energies are found to decrease with the increase of the basis set dimension. The molecular charge distribution of a molecule depends on the dipole moment a vector in three dimensions. Direction of the dipole moment vector in a molecule shows on the center of positive and negative charges. Dipole moments are strictly determined for neutral molecules. For charged systems, its value depends on the choice of origin and molecular orientation. As a result of HF calculations the highest dipole moment was observed for 6-311G+(d,p) whereas the smallest one was observed for B3LYP/6-311+G(d,p) of 4CLPH4CLBENSUL (Table 3).

Table 4: Theoretical electronic absorption spectra of 4CLPH4CLBENSUL, (absorption wavelength λ (nm), excitation energies E (eV) and oscillator strengths (f)) using TD-DFT/B3LYP/6-311++G(d,p) method in gas and solvent (Acetonitrile and DMSO) phase.

Solvents	λ (nm)	E (eV)	(*f*)	Major contribution
Acetonitrile	5.7355	216.17	0.2460	HOMO-2->LUMO (52%)
	5.7382	216.07	0.0407	HOMO-3->LUMO (67%)
	5.8700	211.00	0.0249	HOMO->LUMO+2 (45%)
	5.8929	210.39	0.0000	HOMO->LUMO+3 (54%)
	7.1045	174.51	2.3695	HOMO-3->LUMO+1 (45%)
	7.3621	168.41	0.0798	HOMO-2->LUMO+1 (54%)
	7.3709	168.21	0.1545	HOMO-1->LUMO+3 (34%),
	7.4313	166.84	0.1397	HOMO->LUMO+5 (36%)
	7.4376	166.70	0.9690	HOMO-1->LUMO+2 (34%)
	7.7573	159.83	0.0008	HOMO-2->LUMO+4 (33%)
DMSO	5.7301	216.37	0.2525	HOMO-2->LUMO (53%)
	5.7347	216.30	0.0420	HOMO-3->LUMO (68%),
	5.8653	211.39	0.0251	HOMO->LUMO+2 (45%)
	5.8923	210.42	0.0000	HOMO->LUMO+3 (54%)
	7.0836	175.03	2.3941	HOMO-3->LUMO+1 (46%),
	7.3410	168.89	0.0727	HOMO-2->LUMO+1 (52%)
	7.3456	168.79	0.1666	HOMO-1->L+3 (35%)
	7.4110	167.30	1.1224	HOMO->LUMO+3 (34%)
	7.4313	166.84	0.0216	HOMO->LUMO+5 (42%)
	7.7569	159.84	0.0008	HOMO-2->LUMO+4 (33%)

Table 5: Calculated energy values, chemical hardness, electronegativity and dipole moment of in Acetonitrile and DMSO

TD–DFT/B3LYP/6–311++G(d,p)	Acetonitrile	DMSO
E_{total} (Hartree)	-2000.2761	-2000.2763
E_{HOMO} (eV)	-9.4768	-9.4781
E_{LUMO} (eV)	1.7591	1.7605
$\Delta E_{HOMO–LUMO\ gap}$ (eV)	11.2359	11.2386
$E_{HOMO–1}$ (eV)	-9.9084	-9.9090
E_{LUMO+1} (eV)	2.6208	2.6235
$\Delta E_{HOMO–1–LUMO+1\ gap}$ (eV)	12.5293	12.5325
$E_{HOMO–2}$ (eV)	-9.9084	-10.0817
E_{LUMO+2} (eV)	2.6208	2.7908
$\Delta E_{HOMO–2–LUMO+2\ gap}$ (eV)	12.5293	12.8725
Electronegativity χ (eV)	3.8585	3.8588
Chemical hardness η (eV)	5.6179	5.6193
Dipole moment (Debye)	4.3694	4.3781

On the basis of vibrational analysis at B3LYP/6-311++G(d,p) level, the standard statistical thermodynamic functions: heat capacity (C) entropy (S) and enthalpy changes (ΔH) for the title compound were obtained from the theoretical harmonic frequencies and listed in Table 3. From Table 3, it can be observed that these thermodynamic functions are increasing with temperature ranging from 100 to 1000 K due to the fact that the molecular vibrational intensities increase with temperature [26]. The correlation equations between heat capacities, entropies, enthalpy changes and temperatures were fitted by quadratic formulas, and the corresponding fitting factors (R^2) for these thermodynamic properties are 0.9944, 0.99938 and 0.99814, respectively. In correlations equations the entropy and heat capacity, the cures are finally slightly decreases. But enthalpy curve is finally increased. The corresponding fitting equations are as follows and the correlation graphics of those shows in Fig. 5.

$$C = 3.38441 + 0.19948T - 8.7073x10^{-5}\,T^2 \qquad (R^2 = 0.9944)$$

$$S = 63.60943 + 0.22778T - 5.3388x10^{-5}\,T^2 \qquad (R^2 = 0.99938)$$

$$\Delta H = -2.3337 + 0.03459T + 4.71975x10^{-5}\,T^2 \qquad (R^2 = 0.99814)$$

All the thermodynamic data supply helpful information for the further study on the 4CLPH4CLBENSUL. They can be used to compute the other thermodynamic energies according to relationships of thermodynamic functions and estimate directions of chemical reactions according to the second law of thermodynamics in thermochemical field. Notice: all thermodynamic calculations were done in gas phase and they could not be used in solution.

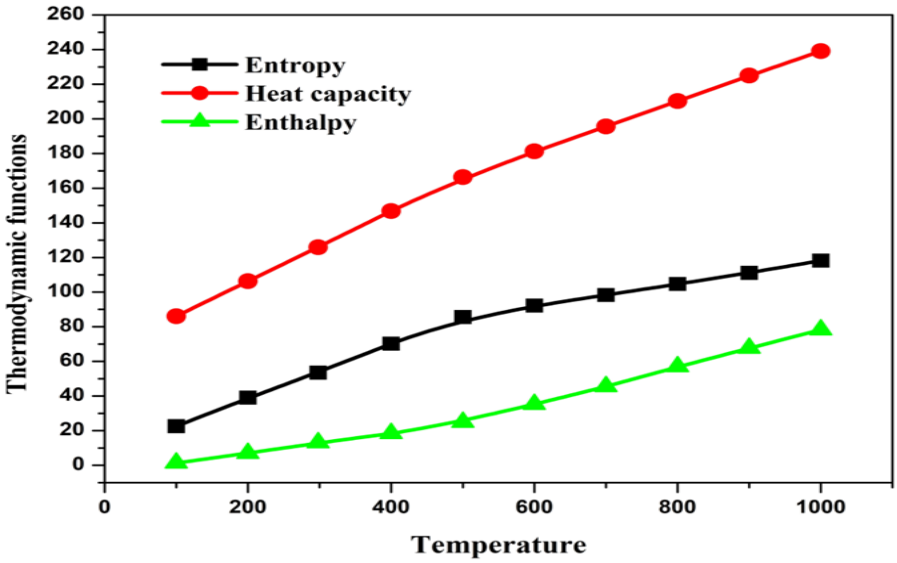

Figure 5: Thermo dynamical graph of 4CLPH4CLBENSUL

4.4 Ultraviolet spectra analysis and Frontier molecular orbitals (FMOs)

The highest occupied molecular orbital (HOMO) and the lowest-lying unoccupied molecular orbitals (LUMO) are named as frontier molecular orbitals (FMOs). The FMOs play an important role in the optical and electric properties, as well as in quantum chemistry and UV–Vis spectra [27]. Gauss-Sum 2.2 Program [28] was used to calculate group contributions to the molecular orbitals (HOMO and LUMO) and prepare the density of the state (DOS) as shown in Fig. 6. The HOMO represents the ability to donate an electron, LUMO as an electron acceptor represents the ability to obtain an electron. The energy gap between HOMO and LUMO determines the kinetic stability, chemical reactivity and, optical polarizability and chemical hardness–softness of a molecule. Chemical hardness and softness can be used as complementary tools in the description of thermodynamic aspects of chemical reactivity.

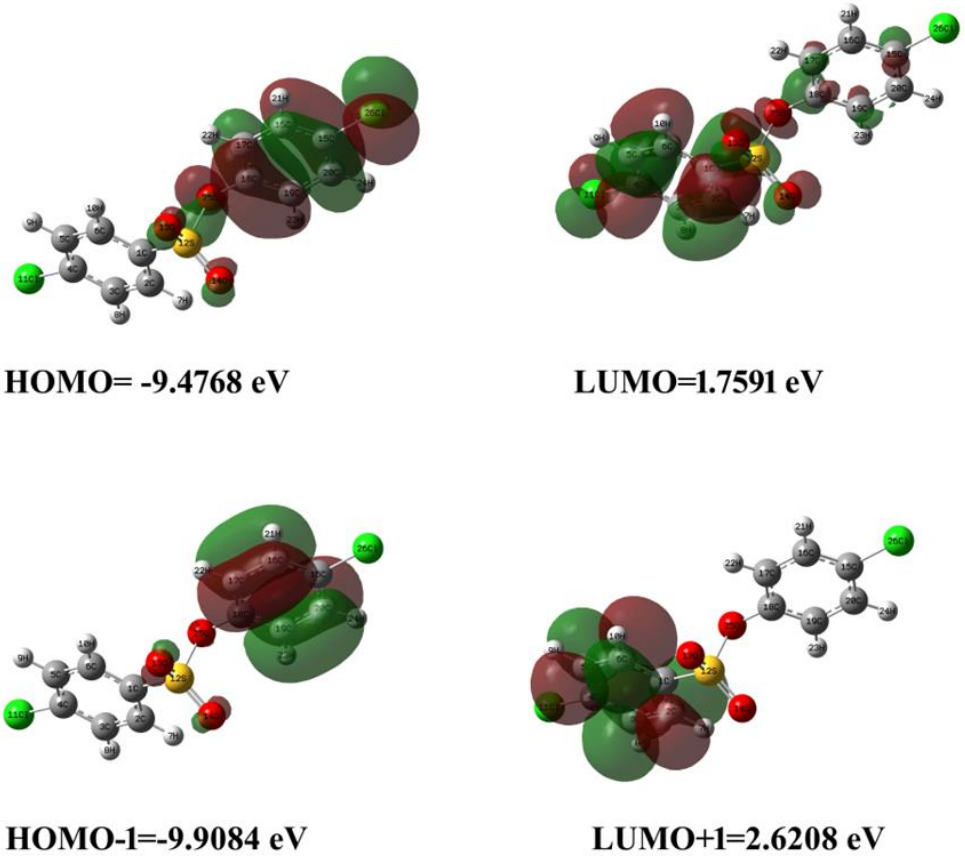

Figure 6: Molecular orbitals and energies for the HOMO and LUMO of 4CLPH4CLBENSULin acetonitrile.

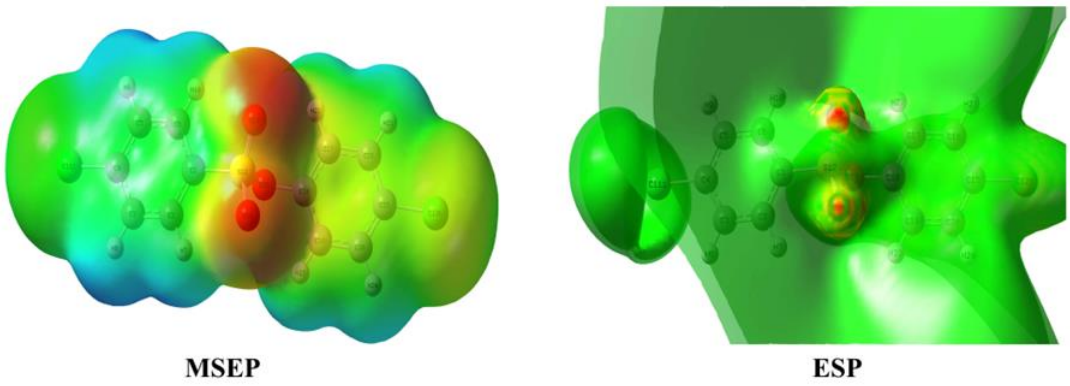

Figure 7: Electrostatic potential (ESP) and the molecular electro static potential (MSEP) map in gas phase of4CLPH4CLBENSUL

In order to evaluate the energetic behavior of the title compound, we carried out calculations in DMSO, chloroform and gas. According to the investigation on FMO energy levels of the title compound, we can find that the corresponding electronic transfer happened between HOMO and LUMO, HOMO and LUMO+1, HOMO and LUMO+2 orbitals, respectively. The energies of four important molecular orbitals for S1 form of 4CLPH4CLBENSUL: the second highest and highest occupied MO's (HOMO, HOMO−1 and HOMO-2), the lowest and the second lowest unoccupied MO's (LUMO, LUMO+1and LUMO+2) were calculated using B3LYP/6-311++G(d,p) and presented in Table 4. The calculated energy value of HOMO is -9.4781 and -9.4768eV in acetonitrile and DMSO, Chloroform and gas, respectively. LUMO is 1.7591 and 1.7605eV in acetonitrile and DMSO, respectively. The value of energy gap between the HOMO and LUMO is 11.2359 and 11.2386 eV in acetonitrile and DMSO, respectively.

The energy gap of HOMO–LUMO explains the eventual charge transfer interaction within the molecule, which influences the biological activity of the molecule. 3D plots of the HOMO and LUMO orbitals computed at the B3LYP/6-311++G(d,p) level for 4CLPH4CLBENSUL molecule are illustrated in Fig. 7 (in gas). The positive phase is red and the negative one is green. It is clear from the figure that, while the HOMO is localized on the whole molecule especially localized on the rings, LUMO is localized on the ring and oxygen atom. The HOMO→LUMO transition implies an electron density transfer. The values of electronegativity, chemical hardness and dipole moment are 3.8588, 5.6193 and4.3781eV in DMSO, respectively, for the title molecule. The dipole moment in a molecule is another important electronic property. For example, the bigger the dipole moment, the stronger will be the intermolecular interactions. The calculated dipole moment values for the molecules are also given in Table 5.

Ultraviolet spectra analyses of 4CLPH4CLBENSUL have been investigated in acetonitrile and DMSO by theoretical calculation. On the basis of fully optimized ground-state structure, TD-DFT/B3LYP/6-311++G(d,p) calculations have been used to determine the low-lying excited states of 4CLPH4CLBENSUL. The theoretical electronic excitation energies, oscillator strengths and absorption wavelength are also listed in Table 7. Calculations of the molecular orbital geometry show that the absorption maxima of this molecule correspond to the electron transition between frontier orbitals such as translation from HOMO to LUMO. As can be seen from Table 5, the calculated absorption maxima values have been found to be 174.51 and 175.03 in acetonitrile and DMSO at DFT/B3LYP/6-311++G(d,p) method. The major contributions of the transitions were designated with the aid of S Wizard program [29].

4.5 Electrostatic potential, total electron density and molecular electrostatic potential

In the present study, a 3D plot of the electrostatic potential (ESP), total electron density (TED) and molecular electrostatic potential (MESP) map of 4CLPH4CLBENSUL is illustrated in Fig. 7. The TED plots for 4CLPH4CLBENSUL molecule show a uniform distribution. However, it can be seen from the ESP figure that while the negative ESP is localized more over nitrogen and oxygen atoms in the molecule and is reflected as a yellowish blob. This result is expected, because ESP correlates with electronegativity and partial charges. The negative electrostatic potential corresponds to an attraction of the proton by the concentrated electron density in the molecule (red colour on the ESP surface), the positive electrostatic potential corresponds to repulsion of the proton by atomic nuclei in regions where low electron density exists and the nuclear charge is incompletely shielded (and shades of blue of colour). The importance of MEP lies in the fact that it simultaneously displays molecular size, shape as well as positive, negative and neutral electrostatic potential regions in terms of colour grading (Fig. 7) and is very useful in research of molecular structure with its physiochemical property relationship [30, 31].

The different values of the electrostatic potential at the surface are represented by different colors. Potential increases in the order red < orange < yellow < green < blue. The color code of these maps is in the range between -0.05710a.u. (deepest red) to 0.05710a.u. (deepest blue) in compound, where blue indicates the strongest attraction and red indicates the strongest repulsion. As can be seen from the MEP map of the title molecule, while regions having the negative potential are over the ring carbon and bromine atoms, the regions having the positive potential are over all hydrogen atoms. Similarly, the ESP is color code in viewing the energy is -0.009873 a.u. to +0.009873 a.u. The front and side view of methyl group in 4CLPH4CLBENSUL is having green colour and it indicates neutral potential. According to these calculated results, the MEP map shows that

the negative potential sites are on nitrogen atoms as well as the positive potential sites are around the hydrogen atom of hydroxyl group.

4.6 Error analysis of different vibrational calculations

The standard deviation is very small in B3LYP/6-311++G(d,p) method. The unscaled theoretical wavenumbers are overestimated and scaled by different scaling factors. This is quite obvious, since calculated frequencies are harmonic in nature, whereas experimental frequencies may involve anharmonicity. In order to reduce the standard deviation between the unscaled and observed fundamentals, overall scale factors are used. The theoretical values in different methods are in harmonic nature. A close agreement between the experimental and scaled wavenumbers is mostly achieved in the fingerprint region. In this, the PM3 method is showed more deviation with the other methods. However, B3LYP method has at the least deviation (14.5391). The relation is usually linear and described by the following equation (x-experimental frequency):

$$\nu_{cal.} = 0.98668\nu_{exp.}\text{-}20.78365\ (R^2 = 0.9991;\ SD=31.03883)\ \text{by HF}$$

$$\nu_{cal.} = 0.36992\nu_{exp.}\ \text{-}1.00084\ (R^2 = 0.9999;\ SD=3.81033)\ \text{by B3LYP}$$

Indicates, the calculated frequencies by B3LYP/6-311++G(d,p) method is exactly fitted with experimental frequencies.

5. Conclusion

A complete vibrational analysis of 4CLPH4CLBENSUL are by performed HF and DFT-B3LYP methods with 6-311++G(d,p) basis set and PM3 method.

Various quantum chemical calculations help us to identify the structural and symmetry properties of the titled molecule. UV-Vis spectral analyses of 4CLPH4CLBENSUL have been analyzed by theoretical calculation.

In order to understand electronic transitions of compound, TD-DFT calculations on electronic absorption spectra in gas phase and solvent (DMSO and chloroform) were performed.

The ESP and MEP maps show the negative potential sites are on oxygen and nitrogen atoms as well as the positive potential sites are around the hydrogen atoms.

Furthermore, the thermodynamic properties of the compound were calculated. The correlations between the statistical thermodynamics and temperature were also obtained.

It was seen that the heat capacity, entropy and enthalpy increase with the increasing temperature owing to the intensities of the molecular vibrations increase with increasing temperature.

References

[1]. Gupta AK, Jain HC, Lynde CW, Macdonald P, Cooper EA, Summerbell RC. Prevalence and epidemiology of onychomycosis in patients visiting physicians' offices: a multicenter Canadian survey of 15,000 patients. J Am Acad Dermatol. 2000 Aug;43(2 Pt 1): 244-248.

[2]. Scher RK, Rich P, Pariser D, Elewski B. The epidemiology, etiology, and pathophysiology of onychomycosis. Semin Cutan Med Surg. 2013 Jun; 32(2 Suppl 1): S2-4.

[3]. Gupta AK, Konnikov N, MacDonald P, Rich P, Rodger NW, Edmonds MW, et al. Prevalence and epidemiology of toenail onychomycosis in diabetic subjects: a multicentre survey. Br J Dermatol. 1998 Oct;139(4):665-71.

[4]. Elewski BE. Onychomycosis: pathogenesis, diagnosis, and management. Clin Microbiol Rev. 1998 Jul;11(3):415-29.

[5]. Hay RJ, Baran R. Onychomycosis: a proposed revision of the clinical classification. J Am Acad Dermatol. 2011 Dec;65(6):1219-27.

[6]. Finch J, Arenas R, Baran R. Fungal melanonychia. J Am Acad Dermatol. 2012 May; 66(5): 830-41.

[7]. Wilsmann-Theis D, Sareika F, Bieber T, Schmid-Wendtner MH, Wenzel J. New reasons for histopathological nail-clipping examination in the diagnosis of onychomycosis. J Eur Acad Dermatol Venereol. 2011 Feb;25(2):235-7.

[8]. Elewski BE, Leyden J, Rinaldi MG, Atillasoy E. Office practice-based confirmation of onychomycosis: a US nationwide prospective survey. Arch Intern Med. 2002 Oct 14; 162(18): 2133-8.

[9]. Onychomycosis: current and future therapies. Cutis. 2014 Feb; 93(2): 60-3.

[10]. Gupta AK, Paquet M, Simpson FC. Therapies for the treatment of onychomycosis. Clin Dermatol. 2013 Sep-Oct; 31(5): 544-54.
[11]. Ghannoum MA, Hajjeh RA, Scher R, Konnikov N, Gupta AK, Summerbell Ret, al. A large-scale North American study of fungal isolates from nails: the frequency of onychomycosis, fungal distribution, and antifungal susceptibility patterns. J Am Acad Dermatol. 2000 Oct; 43(4): 641-8.
[12]. Gu D, Hatch M, Ghannoum M, Elewski BE. Treatment-resistant dermatophytosis: A representative case highlighting an emerging public health threat. JAAD. 2020 November; 6(11):1153-1155.
[13]. Saunte DML, Hare RK, Jorgensen KM, Jorgensen R, Deleuran M, Zachariae CO, et al. Emerging Terbinafine Resistance in Trichophyton: Clinical Characteristics, Squalene Epoxidase Gene Mutations, and a Reliable EUCAST Method for Detection. Antimic Agent and Chemo. 2019 Sept; 63(10).
[14]. Gupta AK, Renaud HJ, Quinlan EM, Shear NH, Piguet V. The Growing Problem of Antifungal Resistance in Onychomycosis and Other Superficial Mycoses. Am J Clin Dermatol. 2021 Mar; 22(2):149-157.
[15]. Astvad KMT, Hare RK, Jørgensen KM, Saunte DML, Thomsen PK, Arendrup MC. Increasing Terbinafine Resistance in Danish Trichophyton Isolates 2019–2020. Journal of Fungi. 2022; 8(2):150.
[16]. Ebert A, Monod M, Salamin K, Burmester A, Uhral ß S, Wiegand C, et al. Alarming India-wide phenomenon of antifungal resistance in dermatophytes: A multicentre study. 2020 Jul; 63(7):717-728.
[17]. Gupta AK, Venkataraman M, Renaud HJ, Summerbell R, Shear NH, Piguet V. A Paradigm Shift in the Treatment and Management of Onychomycosis. Skin Append Disord. 2021;7(5).
[18]. M.J. Frisch et al, Gaussion 03 Program, Gaussian, Inc., Wallingford, CT, 2004.
[19]. A. Frisch, A.B. Nielsen, A.J. Holder, Gaussview Users Manual, Gaussian Inc., Pittsburg.
[20]. R.I. Dennington, T. Keith, J. Millam, K. Eppinnett, W. Hovell, Gauss View Version 3.09, 2003.
[21]. G. Keresztury, S. Holly, J. Varga, G. Besenyei, A.Y. Wang, J.R. Durig, Spectrochim. Acta 9A (1993) 2007-2026.
[22]. G. Keresztury, in: J.M. Chalmers, P.R. Griffith (Eds.), Raman Spectroscopy: Theory, Hand book of Vibrational Spectroscopy, vol. 1, John Wiley & Sons Ltd., New York, 2002.
[23]. H. Fun, K. Chanawannob and S.S uchada Chantrapromm, *Acta Cryst.* (2009). E65, o1554–o1555
[24]. M. Govindarajan, K. Ganasan, S. Periandy, M. Karabacak, S. Mohan, Spectrochim. Acta, A 77 (2010) 1005-1013.
[25]. J. BevanOtt, J. Boerio-Goates, Calculations from Statistical Thermodynamics, Academic Press, 2000.
[26]. I. Fleming, Frontier Orbitals and Organic Chemical Reactions, Wiley, London, 1976.
[27]. N.M.O' Boyle, A.L. Tenderholt, K.M. Langer, J. Comput. Chem. 29(2008) 839-845.
[28]. S.I. Gorelsky, S Wizard Program Revision 4.5, http://www.sg.chem.net/, University of Ottawa, Ottawa, Canada, 2010.
[29]. J.S. Murray, K. Sen, Molecular Electrostatic Potentials, Concepts and 399 Applications, Elsevier, Amsterdam, 1996.
[30]. E. Scrocco, J. Tomasi, in: P. Lowdin (Ed.), Advances in Quantum Chemistry, Academic Press, New York, 1978.
[31]. J. Sponer, P. Hobza, Int. J. Quant. Chem. 57 (1996) 959-970.